Volume 1 | Number 1 | Jan 2013 | Pages 1–100

Journal of
Materials Chemistry A

Materials for energy and sustainability
www.rsc.org/materialsA

ROYAL SOCIETY OF CHEMISTRY

ROYAL SOCIETY OF CHEMISTRY

www.rsc.org/materialsA

1 **Palladium nanoparticles immobilized on core-shell magnetic**

2 **fibrous as highly efficient and recyclable heterogeneous catalyst for**

3 **reduction of 4-nitrophenol and Suzuki coupling reactions**

4 Xuanduong Le,[a] Zhengping Dong,*[a] Yansheng Liu,[a] Zhicheng Jin,[a] Thanh-Do

5 Huy,[b] Minhdong Le[b] and Jiantai Ma*[a]

6 [a]*Gansu Provincial Engineering Laboratory for Chemical Catalysis, College of*

7 *Chemistry and Chemical Engineering, Lanzhou University, Lanzhou 730000, PR*

8 *China.*

9 [b]*Faculty of Technical Physics and Chemistry, Le Quy Don Technical University,*

10 *Hanoi, Vietnam.*

11

12 *∗ Corresponding author, E-mail addresses: dongzhp@lzu.edu.cn (Zhengping Dong),*

13 *majiantai@lzu.edu.cn (Jiantai Ma).*

14 *Tel.: +86 931 891 2311; Fax: +86 931 891 2582.*

15
16
17
18
19
20
21
22
23
24
25
26
27
28
29

1 **Abstract**

2 In this study, a novel core-shell magnetic fibrous nanocatalyst

3 Pd/Fe_3O_4@SiO_2@KCC-1 with easy accessibility of active sites and convenient

4 recovery by applying an external magnetic field was successfully developed.

5 Fe_3O_4@SiO_2@KCC-1 was functionalized with amino groups acting as robust anchors

6 so that the palladium nanoparticles (Pd NPs) with an average diameter of about 4 nm

7 were well-dispersed on the fibers of the Fe_3O_4@SiO_2@KCC-1 without obvious

8 aggregation. The synthesized Pd/Fe_3O_4@SiO_2@KCC-1 nanocatalyst exhibited

9 excellent catalytic activity in the reduction of 4-nitrophenol by sodium borohydride,

10 and Suzuki cross coupling reactions of aryl chlorides with aryl boronic acids due to

11 the easy accessibility of the active sites. Furthermore, the Pd/Fe_3O_4@SiO_2@KCC-1

12 nanocatalyst was conveniently recovered by magnet and could be reused for at least

13 five cycles without significant loss in activity; thus, confirming its good stability.

14 Therefore, the above mentioned approach based on core-shell magnetic fibrous

15 Fe_3O_4@SiO_2@KCC-1 provided a useful platform for the fabrication of Pd NPs based

16 catalysts with easy accessibility, superior activity and convenient recovery.

17

18

19

20

21

22

1. Introduction

In the catalytic area, noble metal nanoparticles (NMNPs) based heterogeneous catalysts have attracted significant attention due to the high catalytic efficiency in numerous liquid-phase catalytic processes.[1-3] In particular, palladium nanoparticles (Pd NPs) based catalysts have been extensively studied because of the superior catalytic performances toward diverse reactions such as Suzuki coupling,[4,5] Heck C-C coupling,[6] degradation of pollutants,[7] hydrogenation,[8] and fuel cells.[9] The catalytic activity of Pd NPs is strongly dependent on the active atoms on the surface that are usually related to the surface properties.[10] Therefore, smaller Pd NPs tends to show a superior catalytic activity as it has a higher surface-to-volume ratio.[11,12] As the size of Pd NPs reduce, the surface energy of Pd NPs increase; thus, leading to a tendency of inter-particle aggregation. The aggregation of Pd NPs will reduce the catalytic efficiency of the catalysts.[13] Therefore, stability of the Pd NPs is another crucial issue for their further application. One solution for Pd NPs stabilization involves the using of appropriate support materials. Various supports such as carbon,[14,15] Al_2O_3,[16,17] mesoporous silica,[18] and core-shell magnetic mesoporous[19] have been used for the immobilization of Pd NPs owing to their excellent stability, high surface areas, and robust surface chemistry. All the above-mentioned materials have large specific surface areas which lead to the great dispersion of the NPs, thus prevent the aggregation of NPs and improve the activity of the catalyst system. However, for all the reported catalysts, poor accessibility to these active sites leads to reduction of the mass transfer effect. Silica supports with easily accessible high surface areas, not due

1 to the pores, therefore, are highly desirable. Vivek Polshettiwar reported the synthesis

2 of fibrous silica nanospheres (KCC-1) by the microwave assisted hydrothermal

3 technique and our laboratory research group reported synthesis of KCC-1 by the

4 hydrothermal method.[20-22] Furthermore, Liu et al. reported the fabrication of

5 core-shell magnetic fibrous $Fe_3O_4@SiO_2@KCC-1$, which both have unique properties

6 of KCC-1 and physical properties of magnetic materials.[23] Therefore, the

7 $Fe_3O_4@SiO_2@KCC-1$ is extremely useful in the design of supported catalysts

8 because of the unique physical properties such as easily accessible of active sites, high

9 surface area, reusability and superparamagnetism.

10 Recently, the transformation of harmful organic wastes into reusable compounds

11 with low toxicity in aqueous solutions under mild conditions has become an

12 extremely important area of study for chemists. As is well known, 4-nitrophenol

13 (4-NP), a well-characterized industrial pollutant which has been listed on the "Priority

14 Pollutant List" by the U.S. Environmental Protection Agency, is harmful to aquatic

15 life and human health in terms of its toxicity, potential carcinogenicity, and

16 mutagenicity.[24-26] The use of catalytic reduction process for the disposal of 4-NP is

17 expected to be the most efficient, green, and economical way.[27, 28] Additionally, much

18 recent work has been directed toward the Suzuki cross coupling reaction because it is

19 the most powerful and widely used method for synthesis of biaryls which are

20 important compounds in pharmaceutical, agrochemical, natural product, and advanced

21 materials chemistry.[29-31] Due to the inherent advantages, several heterogeneous

22 catalysts for Suzuki cross coupling reaction have been developed. Particular attentions

1   are paid to the use of aryl chlorides as substrates because they are much cheaper and

2   readily available than the usually used aryl bromides and iodides. Therefore, the

3   catalytic activity of heterogeneous catalysts for Suzuki cross coupling of aryl

4   chlorides is considerably challenged. So far, heterogeneous examples for the Suzuki

5   cross coupling reaction of less reactive aryl chlorides are quite rare.[32]

6   Based on the aforementioned considerations, herein, we report the synthesis of a

7   novel core-shell magnetic fibrous $Pd/Fe_3O_4@SiO_2@KCC-1$ nanocatalyst system

8   which has the following advantages (Scheme 1). First, the $Pd/Fe_3O_4@SiO_2@KCC-1$

9   nanocatalyst exhibits high accessibility and excellent catalytic activity for reduction of

10 4-NP and Suzuki cross coupling reactions of aryl chlorides with aryl boronic acids.

11 Second, the catalyst could be easily recovered from the reaction mixture by a magnet

12 because of the inner magnetic Fe_3O_4 core. Third, the as-prepared catalyst is long-life,

13 namely, it exhibits high reusability without visibly decrease in the catalytic

14 performance after five cycles. Therefore, this study of $Pd/Fe_3O_4@SiO_2@KCC-1$

15 nanocatalyst system provides a useful platform for exploring environmentally friendly

16 Pd NPs based catalysts with superior activity, convenient recovery, and reusability.

17
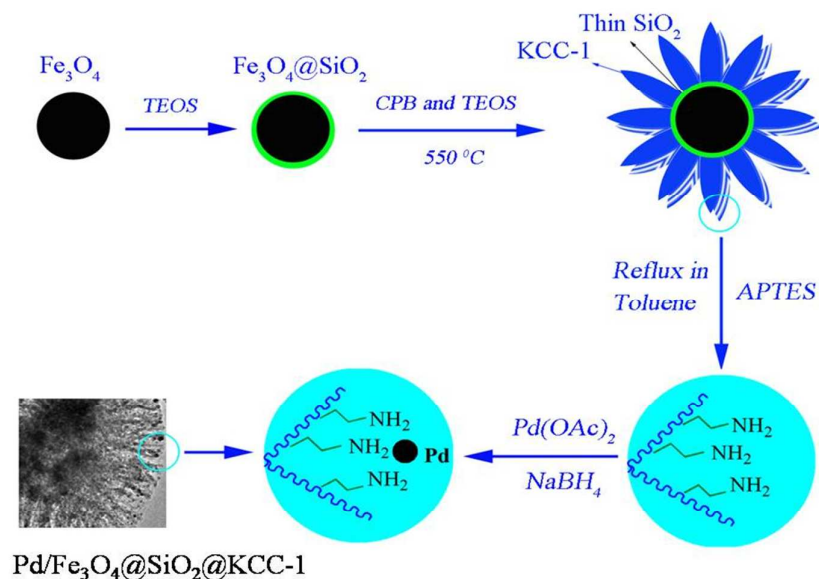
Pd/Fe$_3$O$_4$@SiO$_2$@KCC-1

1

2   **Scheme 1** Preparation of the Pd/Fe$_3$O$_4$@SiO$_2$@KCC-1 nanocatalyst.

3   **2. Experimental section**

4   *2.1. Material*

5   Tetraethoxysilane (TOES), 3-aminopropyltriethoxysilane (APTES), and Pd(II) acetate

6   were purchased from Aladdin Chemical Co., Ltd. 4-NP, 1-pentanol, urea, and aryl

7   halide were purchased from Lanzhou Aihua Chemical Company. Aryl boronic acids

8   were obtained from Shanghai Chemical Reagent Co. Ltd. Organic solvents used were

9   of analytical grade and did not require further purification.

10   *2.2. Synthesis of Fe$_3$O$_4$ and Fe$_3$O$_4$@SiO$_2$ core-shell microspheres*

11   The Fe$_3$O$_4$ NPs and Fe$_3$O$_4$@SiO$_2$ core-shell microspheres were synthesized according

12   to the method reported.[33] FeCl$_3$ (2.6 g, 16 mmol), trisodium citrate (1.0 g, 3.4 mmol),

13   and sodium acetate (NaAc) (4.0 g, 48.8 mmol) were dissolved in ethylene glycol (80

14   mL) with magnetic stirring. The obtained yellow solution was then transferred and

15   sealed into a Teflon-lined stainless-steel autoclave. The autoclave was heated at 200

1 ^{o}C for 10 h, and then allowed to cool to room temperature. The black products were

2 isolated by strong magnetic suction, washed with ethanol and deionized water several

3 times.

4 The $Fe_3O_4@SiO_2$ nano-spheres were prepared through a versatile solution sol-gel

5 method as follows. The Fe_3O_4 NPs (0.7 g) was dispersed to a three-neck

6 round-bottom flask charged with absolute ethanol (140 mL), deionized water (40 mL),

7 and ammonia solution (3 mL, 25%) by ultrasonication for 1 h. Then the mixture was

8 mixed uniformity under mechanical stirring for 15 min at room temperature.

9 Afterward, 2.0 mL TEOS was added dropwise and the mixture was allowed to

10 proceed for 12h under strong mechanical stirring. The resultant core-shell

11 $Fe_3O_4@SiO_2$ nano-sphere product was separated by strong magnetic suction.

12 Followed by washing with ethanol and deionized water several times.

13 *2.3. Syntheis of $Fe_3O_4@SiO_2@KCC$-1 core-shell microspheres*

14 The $Fe_3O_4@SiO_2@KCC$-1 core-shell microspheres were synthesized according to the

15 literature method (scheme 1).[23] $Fe_3O_4@SiO_2$ (0.25 g) was dispersed in an aqueous

16 solution (30 mL) containing urea (0.3 g) to from solution A under ultrasonication 1 h.

17 CPB (0.5 g) was added to 0.75 mL of n-pentanol and 30 mL cyclohexane to from

18 solution B. Solution A was added to solution B under stirring at room temperature.

19 Then 1.25 g TEOS was added dropwise to the above solution. The resulting mixture

20 was continually stirred for 1 h at room temperature and then placed into a 120 ^{o}C

21 environment for 5 h, thus inciting a reaction. After the reaction was completed, the

22 mixture was allowed to cool to room temperature, and the $Fe_3O_4@SiO_2@KCC$-1

1 core-shell microspheres was isolated by strong magnetic suction, washed with

2 deionized water and acetone, and dried overnight in a drying oven at 40 $^{\circ}$C. This

3 material was then calcined at 550 $^{\circ}$C for 5 h in air.

4 *2.4. Preparation of the Pd/Fe$_3$O$_4$@SiO$_2$@KCC-1 nanocatalyst*

5 The aminopropyl functionalized Fe$_3$O$_4$@SiO$_2$@KCC-1 nanocomposite

6 Fe$_3$O$_4$@SiO$_2$@KCC-1-NH$_2$ was synthesized by the following procedures (Scheme 1).

7 In a 100 mL round-bottom flask, Fe$_3$O$_4$@SiO$_2$@KCC-1 (0.6 g) and APTES (0.15 g)

8 were introduced into 50 mL toluene by ultrasonication for 1 h. The mixture was

9 refluxed for 12 h at nitrogen protection. After being cooled to room temperature, the

10 solution was isolated by strong magnetic suction, and the solid was washed several

11 times with ethanol to remove the remaining non-supported APTES. It was then dried

12 in a drying oven at 40 $^{\circ}$C overnight, from which Fe$_3$O$_4$@SiO$_2$@KCC-1-NH$_2$

13 nanocomposites were obtained.

14 Pd/Fe$_3$O$_4$@SiO$_2$@KCC-1 nanocatalyst was synthesized by the following

15 procedures. A 100 mL round-bottom flask was charged with 0.5 g

16 Fe$_3$O$_4$@SiO$_2$@KCC-1-NH$_2$ nanocomposite, 0.1 g Pd(OAc)$_2$, 30 mL deionized water,

17 and 20 mL acetonitrile, after which it was ultrasonically dispersed for 30 min. The

18 obtained suspension was stirred at room temperature for 2 h. Subsequently, the fresh

19 NaBH$_4$ solution (0.2 M, 10 mL) was added into the above-mentioned suspension.

20 After 2 h of reduction, the product was isolated by strong magnetic suction, washed

21 repeatedly with deionized water and ethanol, and dried overnight in a vacuum at 30

22 $^{\circ}$C.

1   *2.5. General procedure for the reduction of 4-NP*

2   The reduction of 4-NP by NaBH$_4$ was chosen as a model reaction for investigation of

3   the catalytic performance of Pd/Fe$_3$O$_4$@SiO$_2$@KCC-1 nanocatalyst. In short, 2.8 mL

4   of deionized water and 30 μL of 4-NP (0.01 M) were mixed with 0.2 mL of freshly

5   prepared aqueous NaBH$_4$ solution (0.5 M), resulting in the formation of a deep yellow

6   solution. Then, 5 μL Pd/Fe$_3$O$_4$@SiO$_2$@KCC-1 nanocatalyst (5 mgmL^{-1}) was added to

7   this resulting solution, and the reaction was allowed to proceed until the solution

8   became colorless. The reaction conversion was determined by the ultraviolet visible

9   spectroscopy (UV-Vis).

10   Reduction reactions were amplified 40X to characterize the reusability of the

11   Pd/Fe$_3$O$_4$@SiO$_2$@KCC-1 nanocatalyst. The catalyst was recovered using a powerful

12   magnet, washed with water and ethanol and dried in a vacuum at room temperature

13   before being used in the next catalytic run. The reduction of 4-NP catalytic process

14   was carried out within 5 min for each cycle. This procedure was repeated five times.

15   *2.6. General procedure for the Suzuki cross coupling reaction*

16   After optimizing the reaction conditions (Table 2), Suzuki coupling reactions were

17   performed by placing aryl halide (0.5 mmol), phenyl boronic acid (0.75 mmol),

18   K$_2$CO$_3$ (1.0 mmol), EtOH (5.0 mL), and Pd/Fe$_3$O$_4$@SiO$_2$@KCC-1 nanocatalyst (0.2

19   mol% Pd) in a 10 mL round bottom flask. The mixture was stirred at 80 °C for

20   required time under air. After the completion of the reaction, the mixture was cooled

21   to room temperature and the Pd/Fe$_3$O$_4$@SiO$_2$@KCC-1 nanocatalyst was separated by

22   powerful magnet. The reaction mixtures were analyzed by Gas chromatography (GC)

1   or GC–mass spectrometry (GC-MS).

2   The recovery and reuse of the Pd/Fe$_3$O$_4$@SiO$_2$@KCC-1 nanocatalyst was

3   described below. A mixture of 1-Iodo-4-nitrobenzene (0.5 mmol), Phenyl boronic acid

4   (0.75 mmol), K$_2$CO$_3$ (1 mmol), EtOH (5.0 mL), and Pd/Fe$_3$O$_4$@SiO$_2$@KCC-1

5   nanocatalyst (0.2 mol% Pd) was stirred at 80 °C under air. After being cooled to room

6   temperature towards the end of the reaction, the Pd/Fe$_3$O$_4$@SiO$_2$@KCC-1

7   nanocatalyst was separated by powerful magnet. The separated catalyst was washed

8   with ethanol and water, respectively, dried under vacuum at room temperature, and

9   reused. The reaction mixtures were analyzed by GC or GC-MS. This procedure was

10   repeated five times.

11   *2.7. Characterization*

12   Powder X-ray diffraction (XRD) spectra were obtained by a Rigaku D/max-2400

13   diffractometer using Cu-Kα radiation in the 2θ range of 10–90°. Fourier transform

14   infrared (FT-IR) spectra were collected on a Nicolet Nexus 670 FT-IR spectrometer

15   equipped with a deuterated triglycine sulfate pyroelectric detector by using KBr

16   pellets. Transmission electron microscopy (TEM) images were obtained on a Tecnai

17   G2 F30, FEI, USA. The UV-Vis measurement was conducted with the UV2800PC

18   UV-Vis spectrophotometer. Magnetic measurement of Fe$_3$O$_4$@SiO$_2$@KCC-1 and

19   Pd/Fe$_3$O$_4$@SiO$_2$@KCC-1 was performed using a quantum design vibrating sample

20   magnetometer (VSM) at room temperature in an applied magnetic field sweeping

21   from −15 to 15 KOe. The reaction conversion was estimated using GC (P.E. Auto

22   System XL) or GC–MS (Shimadzu QP2010S).

3. Results and discussion

3.1. Catalyst preparation and characterization

As can be seen in Scheme 1, $Fe_3O_4@SiO_2@KCC-1$ was first functionalized with APTES, then the aminopropyl groups can be acted as adsorption centers for Pd^{2+}. When the $NaBH_4$ was added to the solution, the Pd^{2+} ions were reduced and immobilized on the fibres of $Fe_3O_4@SiO_2@KCC-1$.

Fig. 1a shows the FT-IR spectra of the $Fe_3O_4@SiO_2@KCC-1$ (black line) and $Fe_3O_4@SiO_2@KCC-1-NH_2$ (red line). The adsorption peaks at 1096 and 805 cm^{-1} correspond to the antisymmetric and symmetric stretching vibration of Si–O–Si bond in oxygen-silica tetrahedron, respectively. The peaks at 467 and 563 cm^{-1} correspond to Si–O, and Fe–O stretching, respectively. The strong peak at 3424 cm^{-1} shows the large number of Si–OH groups which are proved to be advantageous for the modification of APTES on the $Fe_3O_4@SiO_2@KCC-1$ surface by hydrogen bonds.[4] The adsorption peak at 2926 cm^{-1} corresponds to -CH stretching. In the FT-IR spectrum of $Fe_3O_4@SiO_2@KCC-1-NH_2$, the peak around 3400 cm^{-1} represents the adsorption of –OH and –NH_2 groups. The nitrogen, hydrogen, and carbon contents were 0.70%, 0.86%, and 3.20% measured by the elementary analysis, respectively. The FT-IR spectra and elemantary analysis data revealed that the APTES was successfully grafted on the $Fe_3O_4@SiO_2@KCC-1$ surface, thus enabling them to act as robust anchors for metal NPs.

The XRD patterns of the $Fe_3O_4@SiO_2@KCC-1$ and $Pd/Fe_3O_4@SiO_2@KCC-1$ samples are shown in Fig. 1b. The broad peak between 20 and 30° corresponds to

1   amorphous silica, indicating that the silica was successfully coated on the surface of

2   Fe_3O_4 core. The XRD pattern of the $Pd/Fe_3O_4@SiO_2@KCC-1$ shows characteristic

3   peaks of magnetite NPs. The sharp and strong peaks confirm that the products are

4   well crystallized.

5
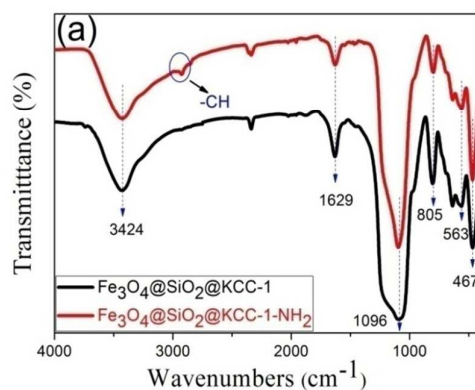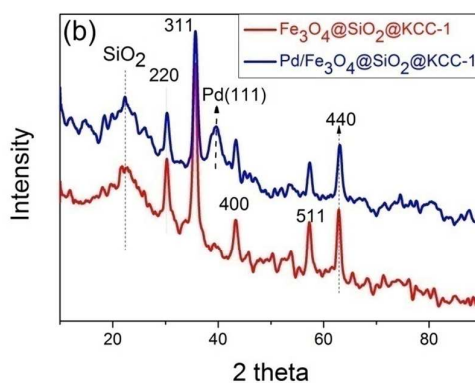
7   **Fig. 1** (a) FT-IR spectra of $Fe_3O_4@SiO_2@KCC-1$ and $Fe_3O_4@SiO_2@KCC-1-NH_2$, (b) The XRD
8   of $Fe_3O_4@SiO_2@KCC-1$ and $Pd/Fe_3O_4@SiO_2@KCC-1$.

9

10   The Fe_3O_4 NPs show five characteristic diffraction peaks at 2 theta = 30.3^o, 35.6^o,

11   43.2^o, 57.2^o, and 63° corresponding to (220), (311), (400), (511) and (440),

12   respectively. The characteristic diffraction peaks at 39.8^o corresponding to Pd (111).

13   The XRD pattern of the $Pd/Fe_3O_4@SiO_2@KCC-1$ demonstrates that the Pd NPs were

14   successfully immobilized on the $Fe_3O_4@SiO_2@KCC-1$ surface. The weight

1   percentage of Pd in the Pd/Fe$_3$O$_4$@SiO$_2$@KCC-1 nanocatalyst, as determined by

2   atomic absorption spectroscopic analysis, were 9.01 wt%.

3   The morphologies and structural features of the core-shell magnetic fibrous

4   Fe$_3$O$_4$@SiO$_2$@KCC-1 and Pd/Fe$_3$O$_4$@SiO$_2$@KCC-1 nanocatalyst were analyzed by

5   TEM. The as-prepared core-shell magnetic fibrous Fe$_3$O$_4$@SiO$_2$@KCC-1 with

6   fibrous structure were uniform and monodispersed (Fig. 2a). As is illustrated in Fig.

7   2a, the Fe$_3$O$_4$@SiO$_2$@KCC-1 possesses the core of Fe$_3$O$_4$ NPs and silica fibres. The

8   average diameter of Fe$_3$O$_4$@SiO$_2$@KCC-1 and the Fe$_3$O$_4$ core were 350 nm and 100

9   nm, respectively. The TEM images shown in Fig. 2b further confirm that the distance

10   between the two fibers is about 18 nm (Fig. 2b). The larger distance between the

11   fibers leads to the easily loading the Pd NPs on Fe$_3$O$_4$@SiO$_2$@KCC-1, resulting in

12   the   significant   increase   in   the   accessibility   of   the   active   sites   on

13   Pd/Fe$_3$O$_4$@SiO$_2$@KCC-1 nanocatalyst. TEM images of Pd/Fe$_3$O$_4$@SiO$_2$@KCC-1

14   nanocatalyst were shown in Fig. 2c. The Pd NPs were remarkably dispersed on the

15   surface of the core-shell magnetic fibrous Fe$_3$O$_4$@SiO$_2$@KCC-1. The Pd NPs have a

16   narrow size distribution with a mean particle size of about 4 nm (Fig. 2c, inset). From

17   the inset picture of Fig. 2c, it can be seen that the resolved lattice fringes of Pd (111)

18   planes (d=0.225 nm) detected in the HRTEM image were attributed to Pd

19   nanocrystals.
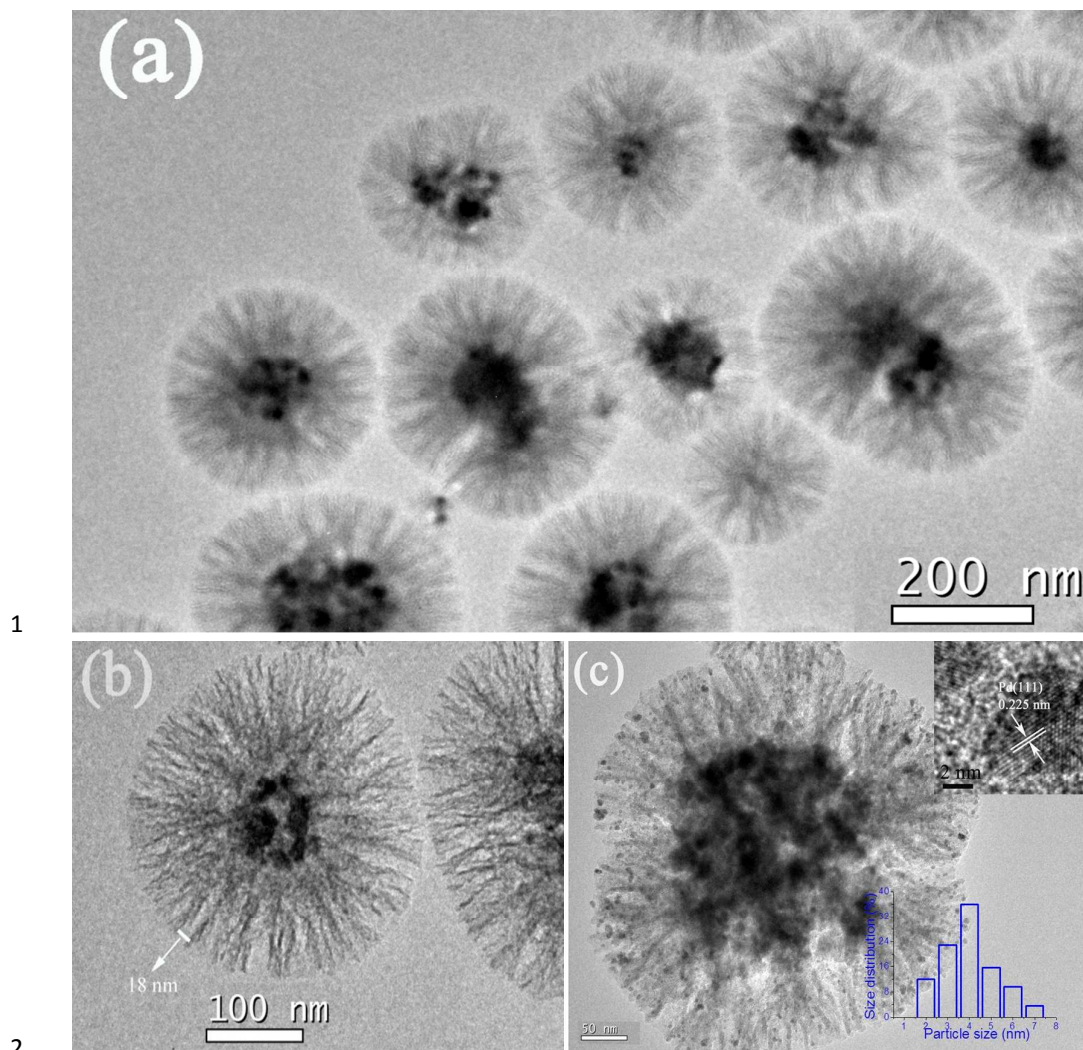
Fig. 2 (a) and (b) TEM images of Fe$_3$O$_4$@SiO$_2$@KCC-1, (c) TEM images of Pd/Fe$_3$O$_4$@SiO$_2$@KCC-1(inset picture; size distribution histogram and HRTEM image of the Pd NPs crystal structure in detail on Fe$_3$O$_4$@SiO$_2$@KCC-1).

The elemental composition of the Pd/Fe$_3$O$_4$@SiO$_2$@KCC-1 samples was determined by EDX analysis and X-ray photoelectron spectroscopy (XPS) (Fig. 3). The EDX spectrum shown in Fig. 3a reveals that the as-prepared products contain Fe, Si, Pd, Cu, C, and O, respectively. Among these elements, Cu and C are generally influenced by the copper network support films and their degree of oxidation; Si, O, Fe and Pd signals result from the Pd/Fe$_3$O$_4$@SiO$_2$@KCC-1 nanocatalyst.
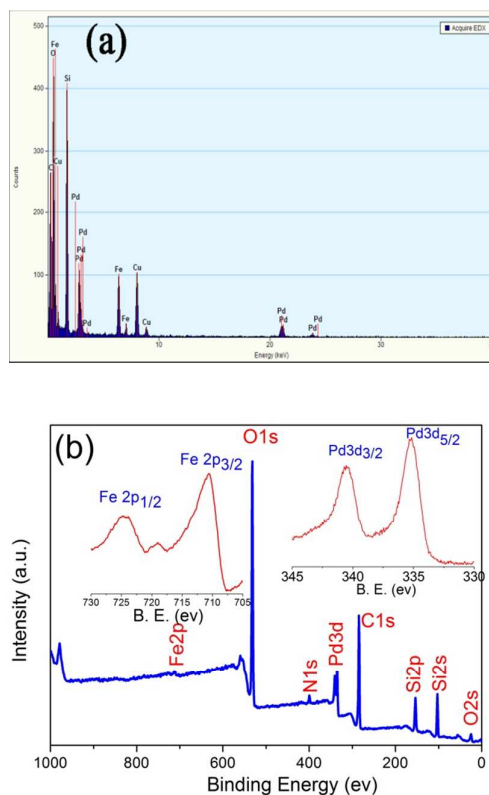
Fig. 3 (a) EDS spectrum of $Pd/Fe_3O_4@SiO_2@KCC$-1, (b) XPS spectrum of $Pd/Fe_3O_4@SiO_2@KCC$-1 (inset image: high resolution spectrum of Fe 2p and Pd 3d)

XPS was performed to investigate the chemical state of the surface of obtained $Pd/Fe_3O_4@SiO_2@KCC$-1 nanocatalyst (Fig. 3b). The XPS elemental survey scan of the surface of $Pd/Fe_3O_4@SiO_2@KCC$-1 nanocatalyst revealed the presence of Si, O, Fe, Pd, N, and C elements in the samples. As shown in Fig. 3b, inset, the peaks observed in the XPS spectra of Fe 2p at binding energies of 711 and 724.5 ev are characteristic of Fe_3O_4. Moreover, the Fig. 3b, inset, also shows the XPS spectrum of Pd $3d_{5/2}$ and Pd $3d_{3/2}$ at binding energies of 335 and 340.5 ev, respectively.

15
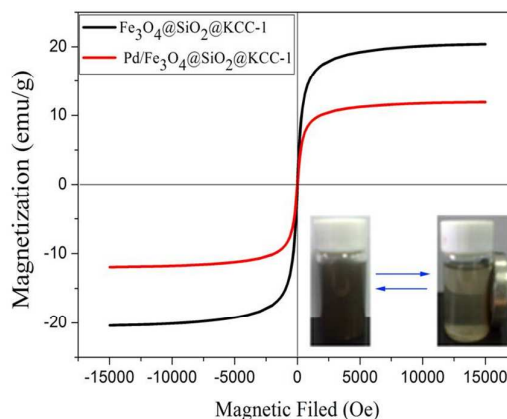
1

2 **Fig. 4** Room temperature magnetization curves of $Fe_3O_4@SiO_2@KCC-1$ and
3 $Pd/Fe_3O_4@SiO_2@KCC-1$ nanocatalyst (inset image: the separation-redispersion process of the
4 $Pd/Fe_3O_4@SiO_2@KCC-1$ nanocatalyst by external magnetic field)

5   Magnetic measurements were carried out by VSM at room temperature. The

6 magnetization curves measured for $Fe_3O_4@SiO_2@KCC-1$ and

7 $Pd/Fe_3O_4@SiO_2@KCC-1$ are shown in Fig. 4. The magnetic saturation values of the

8 $Fe_3O_4@SiO_2@KCC-1$ and $Pd/Fe_3O_4@SiO_2@KCC-1$ are 20.4 and 12 $emug^{-1}$,

9 respectively. The decrease in the saturation magnetization was due to the presence of

10 the APTES and Pd nanoparticles on the $Fe_3O_4@SiO_2@KCC-1$ surface. Moreover, Fig.

11 4 (inset image) shows the separation-redispersion process of the

12 $Pd/Fe_3O_4@SiO_2@KCC-1$ nanocatalyst demonstrating that the catalyst is drawn from

13 the solution to the sidewall of the vial by applying an external magnetic field is

14 removed. Therefore, the abovementioned results indicated an easy and efficient way

15 to separate and recycle the $Pd/Fe_3O_4@SiO_2@KCC-1$ nanocatalyst from the solution

16 by external magnetic field.

17 *3.2. Catalytic reduction for 4-NP*

16

1   The catalytic activity of the Pd/Fe_3O_4@SiO_2@KCC-1 nanocatalyst was studied by

2   reduction reactions of 4-NP to 4-AP in presence of $NaBH_4$. The reduction process was

3   monitored by UV-Vis absorption spectroscopy. As shown in Fig. 5a, pure 4-NP

4   solution exhibited a distinct absorption maximum at 317 nm, which shifts to 400 nm

5   in the presence of alkali because of the formation of 4-nitrophenolate ions.[34] The

6   reduction of 4-NP to 4-AP can be obtained in the presence of $NaBH_4$ without any

7   catalyst, but such required about 430 min.[35]   Furthemore, when the support

8   Fe_3O_4@SiO_2@KCC-1 was added to the 4-NP and $NaBH_4$ solution, it was found that,

9   the color of the reaction mixture did not change even after 120 min, suggesting the

10   Fe_3O_4@SiO_2@KCC-1 support was almost inactive for the reduction reaction (Fig. S1).

11   Because of this, Pd/Fe_3O_4@SiO_2@KCC-1 nanocatalyst was added in order to

12   significantly shorten the reaction time. When the Pd/Fe_3O_4@SiO_2@KCC-1

13   nanocatalyst was added into the reaction mixture, the BH_4^- ions were adsorbed on the

14   surface of Pd NPs and transfer a surface-hydrogen species to the surface of the Pd

15   NPs. Simultaneously, the 4-nitrophenolate were also adsorbed on the surface of the Pd

16   NPs resulting in the rapid occurrence and completion of the reduction reactions.[36, 37]

17   The addition of Pd/Fe_3O_4@SiO_2@KCC-1 nanocatalyst into the reaction mixture led

18   to the decrease in the peak intensity of 4-nitrophenolate ion at 400 nm with the

19   concomitant increase in the peaks corresponding to 4-AP at 300 nm (Fig. 5b) reflects

20   decay of 4-NP and formation of 4-AP. Thus, the conversion of 4-NP to 4-AP can be

21   monitored by tracking the changes in the absorbance peak of 4-nitrophenolate ions at

22   400 nm.[38] When the absorbance peak value of 4-nitrophenolate ions at 400 nm

1   decreased to zero, indicated the successful conversion of 4-NP to 4-AP. Fig. 5b shows

2   completely reduced 4-NP to 4-AP after 275 seconds. The concentration of $NaBH_4$ was

3   very high compared with that of 4-NP, the reaction followed pseudo-first-order

4   reaction kinetics.[22] Therefore, we used pseudo-first-order kinetics to evaluate the

5   kinetic rate constant (k_{app}) of the current reaction[eqn(1)]. The reaction conversion

6   was calculated from C_t/C_0 (Fig. 5c), which was measured using the relative intensity

7   of UV-Vis absorbance (A_t/A_0) at 400nm. C_t and C_0 are the concentrations of the 4-NP

8   at reaction time t and the initial stage, respectively.

9 $$dC_t/dt = -k_{app}t, \text{ or } \ln(C_t/C_0) = \ln(A_t/A_0) = -k_{app}t \quad (1)$$

10   As shown in Fig. 5c, the linear correlation between $\ln(C_t/C_0)$ and reaction time (t)

11   was confirmed through pseudo-first-order kinetics. We calculated the reaction

12   apparent kinetic rate constant k_{app} to be 1.96×10^{-2} for the $Pd/Fe_3O_4@SiO_2@KCC-1$

13   catalyzed reductions of 4-NP. Then, k_{app} was normalized to the concentration of Pd,

14   deriving k_{nor} to reveal the intrisic catalytic activity of the catalyst ($k_{nor}=k_{app}/c_{(Pd)}$).[14] We

15   compared the activity of the $Pd/Fe_3O_4@SiO_2@KCC-1$ with Pd catalysts loaded on

16   different supports for the reduction of 4-NP (Table 1). In Table 1, the

17    $Pd/Fe_3O_4@SiO_2@KCC-1$ shown excellent catalytic activity for the reduction of 4-NP

18   by $NaBH_4$, with the highest k_{nor}(2.78 $s^{-1}mM^{-1}$) among the Pd catalysts loaded on

19   different supports (SBA-15,[39] PEDOT (conducting polymer),[40] Microgel-PS (microgel

20   coated polystyrene),[41] FG (functionalized grapheme nanohybrids), [42]PiHP

21   (hyperbranched polymer)[43], and Al_2O_3.[44] It is also higher than the Pd nanoclusters[45]

22   and Pd nanocrystals[46] based catalysts. The excellent catalytic activity of the

1   Pd/Fe$_3$O$_4$@SiO$_2$@KCC-1 nanocatalyst owes to the ease of access of its active sites,

2   and the low aggregation of the Pd NPs on the Fe$_3$O$_4$@SiO$_2$@KCC-1 support. In this

3   situation, reactant can be easily adsorbed on the Pd NPs surface, which allows the

4   reduction reactions to start quickly and finish rapidly.
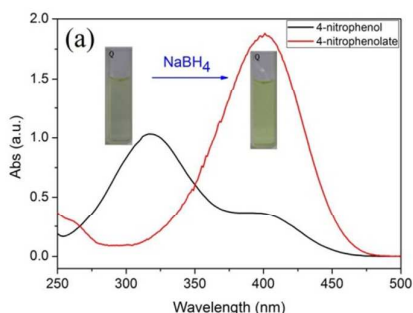
5
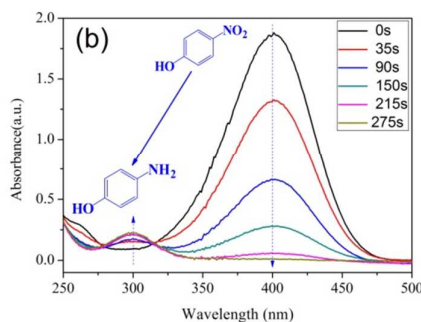
6
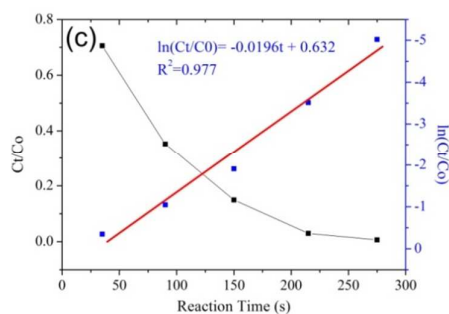
7

8   **Fig. 5** (a) UV-Vis spectra of 4-NP before and after adding NaBH$_4$ solution, (b) the successive

9   reduction of 4-NP to 4-AP over the prepared Pd/Fe$_3$O$_4$@SiO$_2$@KCC-1 nanocatalyst, (c) plost of

10   C$_t$/C$_o$ and ln(C$_t$/C$_o$) versus reaction time for the reduction of 4-NP over Pd/Fe$_3$O$_4$@SiO$_2$@KCC-1.

11

1 **Table 1**

2 Comparison of apparent kinetic rate constant (k_{app}) and normalized rate constants (k_{nor}) of Pd

3 catalysts loaded on different supports for the reduction of 4-NP

Samples	$c_{(4-NP)}(mM)^a$	$c_{(Pd)}(mM)^a$	$k_{app}(s^{-1})^b$	$k_{nor}(s^{-1}\ mM^{-1})^c$	Reference
Pd/SBA-15	0.1	6.29×10^{-2}	11.8×10^{-3}	0.118	[39]
Pd/PEDOT		2.52×10^{-1}	65.8×10^{-3}	0.261	[40]
Pd/Microgel-PS	0.1	2.15×10^{-3}	1.50×10^{-3}	0.698	[41]
Pd/FG	5.8×10^{-2}	4.72×10^{-3}	2.35×10^{-3}	0.498	[42]
Pd nanoclusters	2	1.6	7.89×10^{-4}	0.005	[45]
Pd/PiHP	2.3	9×10^{-2}	20×10^{-3}	0.222	[43]
Pd nanocrystals	8×10^{-2}	3.6×10^{-2}	4.83×10^{-3}	0.134	[46]
Pd/Al$_2$O$_3$	0.1	8.48×10^{-3}	9.2×10^{-3}	1.085	[44]
Pd/Fe$_3$O$_4$@SiO$_2$@KCC-1	0.1	7.06×10^{-3}	19.6×10^{-3}	2.78	This work

4 ^{a}c: concentration. ^{b}k$_{app}$: apparent rate constant. ^{c}k$_{nor}$: rate constant normalized to the molar

5 concentration of Pd. Data were given or calculated in the respective papers; some data were not

6 obtained.

7 *3. 3. Catalyst testing for Suzuki cross coupling reaction.*

8 The above results revealed that the Pd/Fe$_3$O$_4$@SiO$_2$@KCC-1 nanocatalyst exhibited

9 excellent for the reduction of 4-NP. We then further explored the catalytic activity of

10 Pd/Fe$_3$O$_4$@SiO$_2$@KCC-1 nanocatalyst for the Suzuki cross coupling reactions. To

11 explore the optimal reaction conditions, a series of reactions was performed using

12 several times, solvents, bases, and temperature to obtain the best possible combination.

13 Initially, the experiment was performed using Suzuki cross-coupling reaction of

14 1-ido-4-nitrobenzene (0.5 mmol) with phenyl boronic acid (0.75 mmol) in presence of

15 Pd/Fe$_3$O$_4$@SiO$_2$@KCC-1 (0.2% Pd) and 5 mL ethanol in air at 80 ^{o}C for 1 h, 2 h, and

16 3h corresponding products were obtained in the following yields: 91.0%, 94.0%, and

17 97%, respectively (Table 2: entries 1-3). The reaction product was obtained the

18 highest yield for 3 h, so the reaction time of 3 h was chosen. As it is known, solvent

19 plays a crucial role in the rate of Suzuki coupling reactions. When the reactions were

carried out in methyl alcohol, ethyl acetate, deionized water, and acetone under the

same conditions, the products obtained in poor to moderate yields of 85.0%, 79.6%,

27.8%, and 30%, respectively (Table 2: entries 4-7). The reactions were carried out

under similar conditions using different base such as K_2CO_3, CH_3COONa, NaOH, and

$(C_2H_5)_3N$, the yields were 97%, 80.3%, 90.1%, and 80.9%, respectively (Table 2:

entries 3, 8-10). For the reactions at room temperature, 40 ^{o}C, and 60 ^{o}C

corresponding products were obtained in the following yields: 54%, 78.8%, and

90.8%, respectively (Table 2: entries 11-13). The best catalytic activity of the

$Pd/Fe_3O_4@SiO_2@KCC-1$ nanocatalyst was observed using ethanol as solvent, and

K_2CO_3 as base at 80 ^{o}C (Table 2: entry 3).

  After screening the reaction conditions, the catalyst system was studied for the

Suzuki cross coupling reaction of various aryl halides and aryl boronic acids (Table 3).

As listed in Table 3, when the coupling of aryl iodides with aryl boronic acids

proceeded at 80 ^{o}C for 3 h, the corresponding products were obtained in high yields

(Table 3: entries 1-8). The $Pd/Fe_3O_4@SiO_2@KCC-1$ nanocatalyst was also revealed

excellent catalytic activity for the coupling between aryl bromides and aryl boronic

acids the reaction times approached 6 h (Table 3: entries 9-18). However, for the

reactions of 1-bromo-2-nitrobenzene poor yields (Table 3, entries 13 and 18) were

obtained, due to the electron-withdrawing $-NO_2$ group in the *ortho* position. It is

worth noting that aryl iodides and aryl bromides containing electron-donating group,

such as $-CH_3$, $-OH$, $-NH_2$ were found to be the more active than aryl iodides and aryl

bromides containing electron-withdrawing, such as $-NO_2$ (Table 3).

1 **Table 2**

2 The effects of solvent, base and temperature on the Suzuki cross coupling of

3 1-Iodo-4-nitrobenzene with phenyl boronic acid using the Pd/Fe$_3$O$_4$@SiO$_2$@KCC-1 nanocatalyst.

4
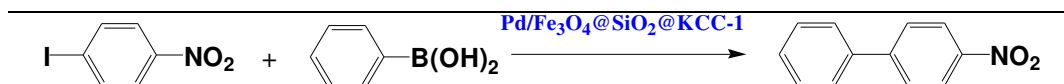
Entry	Solvent	Base	Temp (^{o}C)	Time (h)	Yield (%)
1	Ethanol	K$_2$CO$_3$	80	1	91.0
2	Ethanol	K$_2$CO$_3$	80	2	94.0
3	Ethanol	K$_2$CO$_3$	80	3	97.0
4	Methyl alcohol	K$_2$CO$_3$	80	3	85.0
5	Ethyl acetate	K$_2$CO$_3$	80	3	79.6
6	Deionized water	K$_2$CO$_3$	80	3	27.8
7	Acetone	K$_2$CO$_3$	80	3	30.0
8	Ethanol	CH$_3$COONa	80	3	80.3
9	Ethanol	NaOH	80	3	90.1
10	Ethanol	(C$_2$H$_5$)$_3$N	80	3	80.9
11	Ethanol	K$_2$CO$_3$	25	3	54.0
12	Ethanol	K$_2$CO$_3$	40	3	78.8
13	Ethanol	K$_2$CO$_3$	60	3	90.8

5

6   Although the catalyst was active for aryl iodides and aryl bromides, our main

7 objective was to design a nanocatalyst for the Suzuki coupling of challenging

8 substrates, that is, the Suzuki coupling reactions of aryl chlorides with aryl boronic

9 acids. In our initial at attempts, we used the same optimized conditions for the aryl

10 iodides and aryl bromides, but the products were obtained in low yields.

11

12

13

1 **Table 3**

2 Suzuki cross coupling reactions of aryl halides with aryl boronic acids using

3 Pd/Fe$_3$O$_4$@SiO$_2$@KCC-1 nanocatalyst.
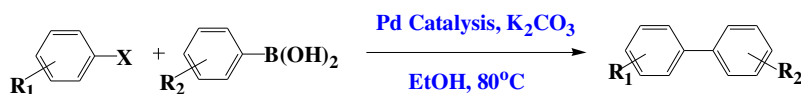
Entry	Aryl halide	Aryl boronic acid	Time (h)	Yield (%)
1	CH$_3$—⬡—I	Cl—⬡—B(OH)$_2$	3	98.9
2	⬡—I	Cl—⬡—B(OH)$_2$	3	96.8
3	HO—⬡—I	Cl—⬡—B(OH)$_2$	3	99.0
4	O$_2$N—⬡—I	Cl—⬡—B(OH)$_2$	3	96.0
5	CH$_3$—⬡—I	⬡—B(OH)$_2$	3	99.0
6	⬡—I	⬡—B(OH)$_2$	3	97.8
7	HO—⬡—I	⬡—B(OH)$_2$	3	99.0
8	O$_2$N—⬡—I	⬡—B(OH)$_2$	3	97.0
9	⬡—Br	Cl—⬡—B(OH)$_2$	6	89.0
10	H$_3$C—⬡—Br	Cl—⬡—B(OH)$_2$	6	91.8
11	H$_2$N—⬡—Br	Cl—⬡—B(OH)$_2$	6	90.6
12	O$_2$N—⬡—Br	Cl—⬡—B(OH)$_2$	6	86.8
13	⬡(NO$_2$)—Br	Cl—⬡—B(OH)$_2$	6	26.2
14	⬡—Br	⬡—B(OH)$_2$	6	90.8
15	H$_3$C—⬡—Br	⬡—B(OH)$_2$	6	93.2
16	H$_2$N—⬡—Br	⬡—B(OH)$_2$	6	91.8
17	O$_2$N—⬡—Br	⬡—B(OH)$_2$	6	87.3
18	⬡(NO$_2$)—Br	⬡—B(OH)$_2$	6	28.1

4 Reaction condition: aryl halide (0.5 mmol), aryl boronic acid (0.75 mmol), K$_2$CO$_3$ (1.0 mmol),

5 EtOH 5.0 mL, Pd/Fe$_3$O$_4$@SiO$_2$@KCC-1 nanocatalyst   (0.2 mol% of Pd), and 80 ^{o}C, in air.

6 Yield was determined by GC-MS or GC analysis.

1 Therefore, we optimized several reaction parameters, including the solvent, reaction

2 temperature and referenced in literatures,[47, 48] and finally found that the use of

3 tetra-n-butylammonium bromide (TBAB) and changed the solvent from ethanol to

4 (n-methyl-2-pyrrolidone) NMP and raised the reaction temperature to 140 $^{\circ}$C was

5 necessary to achieved good yields. After optimizing the reaction conditions, the

6 Pd/Fe_3O_4@SiO_2@KCC-1 nanocatalyst was studied for Suzuki cross coupling

7 reactions of several aryl chlorides with aryl boronic acids, which are summarized in

8 Table 4.

9 **Table 4**
10 The Suzuki cross coupling reactions of aryl cholorides with aryl boronic acids using
11 Pd/Fe_3O_4@SiO_2@KCC-1 nanocatalyst.

12

Entry	Aryl cholorides	Aryl boronic acid	Time (h)	Yield (%)
1			12	83.2
2			12	86.0
3			12	85.8
4			12	80
5			12	83.8
6			12	87.8
7			12	86.2
8			12	79.8

Reaction condition: aryl cholorides (0.5 mmol), aryl boronic acid (0.75 mmol), K_2CO_3 (1.0 mmol) were added in 5 ml NMP at 140 $^{\circ}$C for 12 h in the presence of TBAB (0.05 mmol) and Pd/Fe_3O_4@SiO_2@KCC-1 (2.5 mol% of Pd). Yield was determined by GC-MS or GC.

1   Interestingly, the Pd/Fe$_3$O$_4$@SiO$_2$@KCC-1 nanocatalyst was also revealed

2   excellent catalytic activity for the Suzuki coupling between aryl chlorides and aryl

3   boronic acids. The highly dispersed smaller Pd NPs and easy accessibility of active

4   sites, as few heterogeneous catalyst systems show good activity toward aryl chlorides,

5   which are sustainable substrates for Suzuki cross coupling reactions, under ligand-free

6   condition.[49]

7   *3.4. Reusability of the Pd/Fe$_3$O$_4$@SiO$_2$@KCC-1 nanocatalyst.*

8   For practical application of heterogeneous systems, the recyclability of catalyst is an

9   important factor. The stability and reusability of the Pd/Fe$_3$O$_4$@SiO$_2$@KCC-1

10   nanocatalyst were performed by catalyzed the reduction of 4-NP and Suzuki coupling

11   reaction of 1-Iodo-4-nitrobenzene with Phenyl boronic acid.
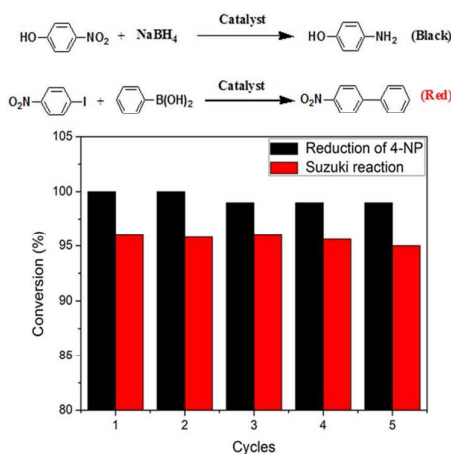
12

13   **Fig. 6** The reusability of Pd/Fe$_3$O$_4$@SiO$_2$@KCC-1 nanocatalyst for the reduction of 4-NP by
14   NaBH$_4$ and Suzuki cross coupling reaction of 1-iodo-4-nitrobenzene with phenyl boronic acid.

15   As shows in Fig. 6, the recovered Pd/Fe$_3$O$_4$@SiO$_2$@KCC-1 nanocatalyst exhibited

16   almost constant catalytic activity for at least five successive cycles in the reduction of

1 4-NP and Suzuki cross coupling reaction of 1-iodo-4-nitrobenzene with Phenyl

2 boronic acid. Moreover, the catalyst was easily separated magnetically from the

3 reaction mixture, washed with ethanol and deionized water, and finally dried for the

4 next run. This result suggests that the Pd/Fe$_3$O$_4$@SiO$_2$@KCC-1 nanocatalyst

5 possesses robust stability.

6 **4. Conclusion**

7 In this study, a novel core-shell magnetic fibrous Fe$_3$O$_4$@SiO$_2$@KCC-1 based

8 Pd/Fe$_3$O$_4$@SiO$_2$@KCC-1 nanocatalyst with easy accessibility of the active sites was

9 successfully synthesized. The catalyst could be easily recovered by applying an

10 external magnetic field, and reused for next catalytic run. The

11 Pd/Fe$_3$O$_4$@SiO$_2$@KCC-1 nanocatalyst showed excellent catalytic activity for the

12 reduction of 4-NP and Suzuki coupling reaction of a range of aryl bromides and

13 iodides with aryl boronic acids. Notably, the catalyst was also displayed good

14 catalytic activity for Suzuki coupling reaction of aryl cholorides with aryl boronic

15 acids. Moreover, the catalyst was chemically stable and could be easily recycled for at

16 least five times in the corresponding reaction without reduction in the catalytic

17 activity. The Pd/Fe$_3$O$_4$@SiO$_2$@KCC-1 nanocatalyst acts as relatively green,

18 superparasitism, eco-friendly nature and convenient recovery, and as a promising

19 candidate for Pd NPs based catalytic applications in industrial synthesis.

References

1. S. Paganelli, O. Piccolo, F. Baldi, R. Tassini, M. Gallo and G. La Sorella, *App. Catal. A: Gen.*, 2013, **451**, 144-152.

2. Y. Shiraishi, K. Fujiwara, Y. Sugano, S. Ichikawa and T. Hirai, *ACS Catal.*, 2013, **3**, 312-320.

3. K. Imamura, T. Yoshikawa, K. Nakanishi, K. Hashimoto and H. Kominami, *Chem. Commun.*, 2013, **49**, 10911-10913.

4. X. Le, Z. Dong, Z. Jin, Q. Wang and J. Ma, *Catal. Commun.*, 2014, **53**, 47-52.

5. P. Wang, H. Liu, J. Niu, R. Li and J. Ma, *Catal. Sci. Technol.*, 2014, **4**, 1333-1339.

6. F. Zhang, J. Jin, X. Zhong, S. Li, J. Niu, R. Li and J. Ma, *Green. Chem.*, 2011, **13**, 1238-1243.

7. M.-Q. Yang, X. Pan, N. Zhang and Y.-J. Xu, *Crystengcomm*, 2013, **15**, 6819-6828.

8. Z. Dong, X. Le, C. Dong, W. Zhang, X. Li and J. Ma, *Appl. Catal. B: Environ.*, 2015, **162**, 372-380.

9. E. Antolini, *Energ. Environ. Sci.*, 2009, **2**, 915-931.

10. H. Lee, S. E. Habas, S. Kweskin, D. Butcher, G. A. Somorjai and P. Yang, *Angew. Chem. Int. Ed.*, 2006, **45**, 7824-7828.

11. J. Zeng, Q. Zhang, J. Chen and Y. Xia, *Nano letters*, 2009, **10**, 30-35.

12. M.-L. Wang, T.-T. Jiang, Y. Lu, H.-J. Liu and Y. Chen, *J. Mater. Chem. A*, 2013, **1**, 5923-5933.

13. Y. Lin, Y. Qiao, Y. Wang, Y. Yan and J. Huang, *J. Mater. Chem.*, 2012, **22**, 18314-18320.

14. Y. Fang and E. Wang, *Nanoscale*, 2013, **5**, 1843-1848.

15. D. Ganapathy and G. Sekar, *Catal. Commun.*, 2013, **39**, 50-54.

16. G. Feng, F. Liu, C. Lin, W. Li, S. Wang and C. Qi, *Catal. Commun.*, 2013, **37**, 27-31.

17. G. Yuan and M. A. Keane, *Ind. Eng. Chem. Res.*, 2007, **46**, 705-715.

18. S. Wei, Z. Ma, P. Wang, Z. Dong and J. Ma, *J. Mol. Catal. A: Chem.*, 2013, **370**, 175-181.

19. W. Li, B. Zhang, X. Li, H. Zhang and Q. Zhang, *Appl. Catal. A: Gen.*, 2013, **459**, 65-72.

20. V. Polshettiwar, D. Cha, X. Zhang and J. M. Basset, *Angew. Chem. Int. Ed.*, 2010, **49**, 9652-9656.

21. A. Fihri, M. Bouhrara, U. Patil, D. Cha, Y. Saih and V. Polshettiwar, *ACS Catal.*, 2012, **2**, 1425-1431.

22. Z. Dong, X. Le, X. Li, W. Zhang, C. Dong and J. Ma, *Appl. Catal. B: Environ.*, 2014, **158–159**, 129-135.

23. K. Yu, X. Zhang, H. Tong, X. Yan and S. Liu, *Mater. Lett.*, 2013, **106**, 151-154.

24. Y. C. Chang and D. H. Chen, *J. Hazard. Mater.*, 2009, **165**, 664-669.

25. J.-R. Chiou, B.-H. Lai, K.-C. Hsu and D.-H. Chen, *J. Hazard. Mater.*, 2013, **248**, 394-400.

26. K. Li, Z. Zheng, X. Huang, G. Zhao, J. Feng and J. Zhang, *J. Hazard. Mater*, 2009, **166**, 213-220.

27. Y. Zhang, X. Yuan, Y. Wang and Y. Chen, *J. Mater. Chem.*, 2012, **22**, 7245-7251.

1   28.   S. Saha, A. Pal, S. Kundu, S. Basu and T. Pal, *Langmuir*, 2010, **26**, 2885-2893.

2   29.   N. Miyaura and A. Suzuki, *Chem. Rev.*, 1995, **95**, 2457-2483.

3   30.   A. Suzuki, *J. Organomet. Chem.*, 1999, **576**, 147-168.

4   31.   P. Wang, F. Zhang, Y. Long, M. Xie, R. Li and J. Ma, *Catal. Sci. Technol.*, 2013, **3**,
5   1618-1624.

6   32.   H. Yang, G. Li and Z. Ma, *J. Mater. Chem.*, 2012, **22**, 6639-6648.

7   33.   Y. Deng, Y. Cai, Z. Sun, J. Liu, C. Liu, J. Wei, W. Li, C. Liu, Y. Wang and D. Zhao, *J. Am.*
8   *Chem. Soc*, 2010, **132**, 8466-8473.

9   34.   K. Kim, K. L. Kim and K. S. Shin, *J. Phys. Chem. C*, 2011, **115**, 14844-14851.

10   35.   T. Wu, L. Zhang, J. Gao, Y. Liu, C. Gao and J. Yan, *J. Mater. Chem. A*, 2013, **1**,
11   7384-7390.

12   36.   B. Baruah, G. J. Gabriel, M. J. Akbashev and M. E. Booher, *Langmuir*, 2013, **29**,
13   4225-4234.

14   37.   D. H. Lee, S. O. Kim and W. J. Lee, *J. Phys. Chem. C*, 2010, **114**, 8114-8114.

15   38.   X. Le, Z. Dong, W. Zhang, X. Li and J. Ma, *J. Mol. Catal. A: Chem.*, 2014, **395**, 58-65.

16   39.   J. Morere, M. J. Tenorio, M. J. Torralvo, C. Pando, J. A. R. Renuncio and A. Cabanas, *J.*
17   *Supercrit. Fluid.*, 2011, **56**, 213-222.

18   40.   S. Harish, J. Mathiyarasu, K. L. N. Phani and V. Yegnaraman, *Catal. Lett.*, 2009, **128**,
19   197-202.

20   41.   Y. Mei, Y. Lu, F. Polzer, M. Ballauff and M. Drechsler, *Chem. Mater.*, 2007, **19**,
21   1062-1069.

22   42.   Z. Wang, C. Xu, G. Gao and X. Li, *Rsc. Adv.*, 2014, **4**, 13644-13651.

23   43.   H. Li, L. Han, J. Cooper-White and I. Kim, *Green. Chem.*, 2012, **14**, 586-591.

24   44.   S. Arora, P. Kapoor and M. Singla, *Reac. Kinet. Mech. Cat.*, 2010, **99**, 157-165.

25   45.   A. Halder, S. Patra, B. Viswanath, N. Munichandraiah and N. Ravishankar, *Nanoscale*,
26   2011, **3**, 725-730.

27   46.   G. Fu, X. Jiang, L. Ding, L. Tao, Y. Chen, Y. Tang, Y. Zhou, S. Wei, J. Lin and T. Lu, *Appl.*
28   *Catal. B: Environ.*, 2013, **138–139**, 167-174.

29   47.   A. Fihri, D. Cha, M. Bouhrara, N. Almana and V. Polshettiwar, *Chemsuschem*, 2012, **5**,
30   85-89.

31   48.   A. Indra, C. S. Gopinath, S. Bhaduri and G. Kumar Lahiri, *Catal. Sci. Technol.*, 2013, **3**,
32   1625-1633.

33   49.   A. Fihri, M. Bouhrara, B. Nekoueishahraki, J.-M. Basset and V. Polshettiwar, *Chem. Soc.*
34   *Rev.*, 2011, **40**, 5181-5203.

35

Pd/Fe$_3$O$_4$@SiO$_2$@KCC-1